Comparing Two Intervals of Exceptionally Strong Solar Rotation Recurrence of Galactic Cosmic Rays

A. Gil[1,2] and K. Mursula[2]

[1]Institute of Mathematics and Physics, Faculty of Scienice, Siedlce University, Siedlce, Poland, [2]ReSoLVE Centre of Excellence, Space Climate Research Unit, University of Oulu, Oulu, Finland

Abstract Two intervals of exceptionally strong recurrence of galactic cosmic ray (GCR) intensity at solar rotation period stand out in recent history, one in 2007–2008 and the other in 2014–2015. We use neutron monitor data from Oulu and Hermanus, solar wind (SW) data, and coronal images to study these intervals. We find that in both cases the source of solar rotation period recurrence was a coronal hole (CH), but CH structures were different. While a large, longitudinally asymmetric CH existed at high southern latitudes in 2014–2015, a low-latitude CH caused the recurrence in 2007–2008. Spectral properties of GCR and SW parameters reflect these differences. In 2014–2015 the GCR power spectrum density was broad and peaked at a period of 28.9 days, longer than the simultaneous recurrence period of SW speed. In 2007–2008 the GCR power spectrum was narrow and peaked at 27.5 days, exactly the same as for SW speed. The effect of CHs to GCRs was somewhat different in the two cases because of opposite solar polarities in the two intervals. In 2014–2015, during positive polarity when GCRs drift inward from high latitudes, the convection of fast SW from CH reduces the inward GCR drift over a wide range of high heliolatitudes at certain heliolongitudes. In 2007–2008, during negative polarity when GCRs drift inward via the heliospheric current sheet, a low-latitude CH depletes the GCR flux not only by convection but also by the deflecting heliospheric current sheet away from the ecliptic, whence GCR drift to higher latitudes in a limited longitude range.

1. Introduction

Galactic cosmic rays (GCR) have been measured on the ground by the worldwide network of neutron monitors (NMs; Simpson, 2000), as well as by several space probes like ACE (Stone et al., 1998) and PAMELA (Picozza et al., 2007). GCR fluxes are modulated by solar activity variations, especially by the solar cycle (Parker, 1956), and by the solar rotation period (Monk & Compton, 1939). Solar rotation is differential, that is, the higher the heliolatitude, the slower the rotation rate is. There are still many open issues about the solar differential rotation, such as its dependence on the level of solar activity and the north-south asymmetry of differential rotation (Suzuki, 2014; Zhang et al., 2013). Investigation of the recurrence of GCR intensity at solar rotation can help to shed some light on those topics.

The analysis of solar parameters during the long minimum between solar cycle (SC) 23 and SC 24, when enhanced GCR recurrence at solar rotation was observed, shows that their values differ significantly from those measured in previous solar minima. The Sun was then extremely quiet, and solar wind (SW) density was lower by about ∼ 30% during this minimum than during the three previous minima (Jian et al., 2011). The heliospheric magnetic field (HMF) and the SW dynamic pressure were also exceptionally weak during the latest minimum (McComas et al., 2008). Hoeksema (2010) concluded that the low values of SW density, velocity, and dynamic pressure may be caused by the SW emerging from the coronal holes (CHs) located close to the equator, while polar CHs were smaller than in previous cycles. Abramenko et al. (2010) found that the area occupied by the near-equatorial CHs within $\pm40°$ of heliolatitude in the recent minimum was larger than in the previous minimum. The weakening of polar fields and the small area of polar CHs during the late declining to the minimum phase of SC 23 are incomparable to previous cycles. The intensity of cosmic rays, as measured by neutron monitors, was highest ever recorded (e.g., Bazilevskaya et al., 2014; Mewaldt et al., 2010; Moraal & Stoker, 2010). The main drivers of the recurrent variation of cosmic rays are the corotating interaction regions (CIRs; Richardson, 2004), where a fast SW stream catches the slow stream (Kunow et al., 1991). Only few epochs are known when the solar rotation periodicity of GCR is very clear. This was the case, for example, in 2007–2008, close to the minimum of SC 23 (Leske et al., 2011; Modzelewska & Alania, 2013).

The variation of GCR intensity at solar rotation period was also very strong in 2014, after the maximum of solar cycle 24 (Singh & Badruddin, 2017). Lario and Roelof (2007) compared the first and third Ulysses passes over the southern part of the heliosphere and found persistent GCR recurrence during the first pass (declining phase of SC 22), but during the third pass (declining phase of SC 23) the latitudinal recurrence structure was less systematic. Based on Ulysses observations Dunzlaff et al. (2008) reported that GCR recurrence due to fast SW had a maximum around 25° of heliographic latitude and was visible up to 40°, whereas in SC 23 the GCR recurrence in fast SW practically disappeared. They suggested that the absence of large polar CHs in SC 23 (e.g., Kirk et al., 2009) may be the reason for this dissimilarity.

Dunzlaff et al. (2008) presented clear anticorrelation between SW speed and cosmic rays, confirming the local effect of convection. Guo and Florinski (2014) used stochastic modeling of the 27-day variation of GCR intensity (for 0.4 GeV galactic protons) and found a relative recurrence of about 3% during the recent solar minimum and a significant role of corotating interaction regions for GCR modulation. Modzelewska and Alania (2013) showed that the period of 27-day variation of GCR intensity was stable in 2007–2008 but changed to a longer period (up to 33–36 days) in 2009.

Here we study GCR intensity variations in 2014–2015 (Carrington rotations 2154–2162: from now on called *Interval A*) and 2007–2008 (Carrington rotations [CRs] 2061–2073: *Interval B*), during the two periods, when solar rotation-related variability in GCR was strongest in the recent history. The paper is organized as follows: in section 2 we present the data used in this paper. In section 3 we study GCR by wavelet and other spectral analysis methods. In section 4 we calculate the amplitudes and phases of solar rotation-related GCR recurrence during the two intervals. Section 5 presents the wavelet coherence analysis. In section 6 we discuss the obtained results and in section 7 give our conclusions.

2. Data

We use daily NM count rates from two stations at greatly different latitudes and in opposite hemispheres: Oulu (OULU; latitude 65.05°N; effective vertical cutoff rigidity of 0.8 GV) and Hermanus (HRMS; 34.25°S; 4.58 GV), which have different sensitivities to the low-energy part of the GCR spectrum and, hence, measure different levels of heliospheric modulation. Figures 1a and 1b present the 5-day running means of daily count rates from Oulu and Hermanus NMs in 2014–2015 (CRs 2146–2172). Figures 2a and 2b present data for the same stations in 2007–2008 (CRs 2052–2078).

Cosmic rays are modulated by solar activity, and we use here the standard measure of solar activity, the sunspot number (SSN). Since the main drivers of the cosmic ray recurrence are CIRs, we also analyze the main SW parameters, SW velocity, the strength of the heliospheric magnetic field, and its radial Bx component. These parameters are included in the OMNI-2 database and reflect the SW conditions at the helioequator. Figures 1c–1f and 2c–2f display the SW velocity (Vsw), HMF strength (B), HMF Bx component, and sunspot number.

Figures 1a and 1b show that the recurrence at solar rotation period in cosmic rays intensity was clearly visible from September 2014 (CR 2155) to February 2015 (CR 2161). Recurrence was somewhat disturbed by transients like Forbush decreases and solar flares (Kraaikamp & Verbeeck, 2015; Lingri et al., 2016) but is clearly noticeable. The periodicity of GCR started at the same time when SW velocity was elevated to a higher level, reflecting the occurrence of fast SW. Rotational variation of SW velocity was also slightly enhanced. HMF strength also increased slightly, mainly due to large spikes related to CIRs, but recurrence was not well manifested. It seems that GCR intensity covariates better with Vsw than HMF strength. HMF Bx component indicates the HMF sector structure, depicting a dominant two-sector pattern at this time. In sunspot number the 27-day recurrence started to be noticeable already in April 2014 (CR 2150) and again in April 2015 (CR 2163), with different periods in between.

Figure 2 presents the time series of cosmic rays intensity and other parameters in Interval B (2007–2008, CRs 2052–2078). In GCR intensity a notable solar rotation recurrence was seen from September 2007 (CR 2061) to July 2008 (CR 2073). In SW velocity this recurrence started to dominate the variability already in March 2007 (CR 2055) and lasted, almost uninterrupted, until November 2008 (CR 2077). HMF Bx component demonstrated a dominant two-sector pattern from July 2007 (CR 2059) until April 2008 (CR 2069).
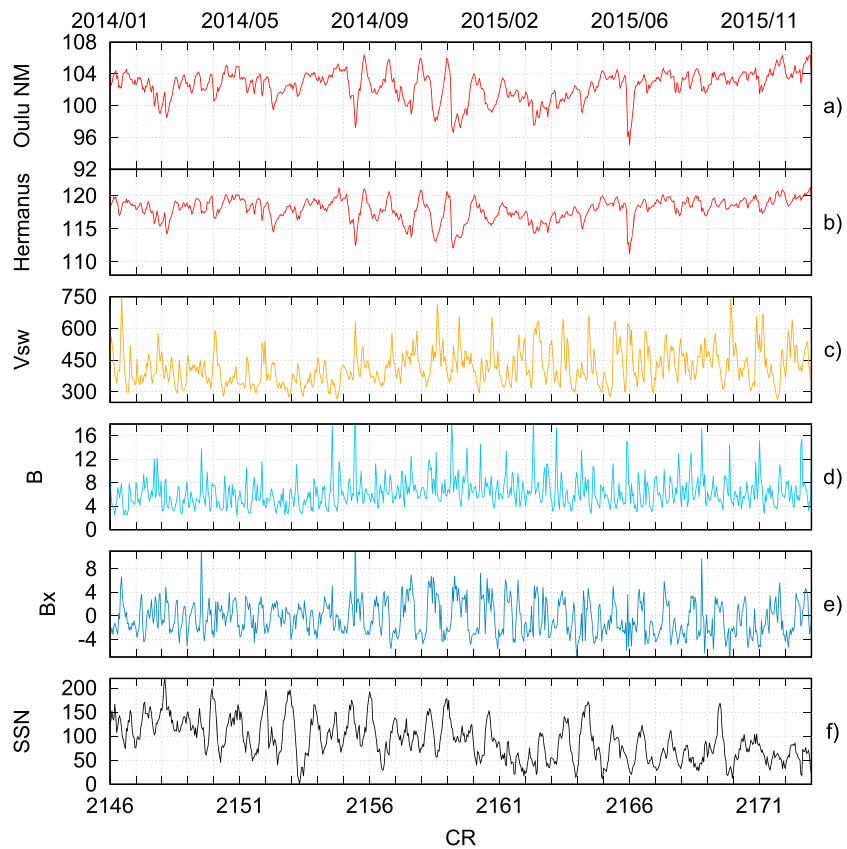
Figure 1. Five-day running means of daily (a) Oulu and (b) Hermanus cosmic ray NM count rates; (c) solar wind velocity (Vsw); (d) strength of the heliospheric magnetic field (*B*); (e) HMF Bx component; and (f) sunspot number (SSN) in 2014–2015 (CRs 2146–2172). Time is given in Carrington rotations (CR) below and in calendar months above. NM = neutron monitors; HMF = heliospheric magnetic field.

3. Filter, Wavelet, and Spectral Analysis

In order to study the strength of the GCR recurrence, we applied a bandpass filter (e.g., Kanasewich, 1981; Shenoi, 2005) to the daily NM data in 2005–2016. Since the solar rotation is differential and we want to include periodicities originating from both equatorial and polar regions, we use a rather wide filter passing 24–34 days (the second-order Butterworth filter). Figure 3 shows the filtered amplitude of Oulu NM in 2005–2016. It is clear that this variability was indeed the strongest at the end of 2014, even stronger than during the solar minimum of 2007–2008.

Next, we used a wavelet analysis (Torrence & Compo, 1998) to further study GCR variability connected with solar rotation. Figure 4 presents the results of wavelet analysis for some of above mentioned parameters, that is, GCR intensity, Vsw, and HMF strength. Figure 4a reveals strong solar rotation variability in Oulu NM data, over a wide period range, from August 2014 (CR 2154) to February 2015 (CR 2161). Figure 4c shows that the solar rotation recurrence appeared in SW velocity slightly later, around October 2014 (CR 2156), and was limited to a more narrow period range than for NM. Figure 4e shows that the solar rotation recurrence in HMF strength was rather weak. However, shorter periodicities, especially the third and the forth harmonics of the solar rotation period, were quite strong.

Figure 4b presents very strong solar rotation recurrence in Oulu NM data from September 2007 (CR 2061) to July 2008 (CR 2072) and weaker even thereafter. It is worth noting that the solar rotation period of about 27 days was very stable during this time. Figure 4d shows that this recurrence also appeared strongly in SW velocity. It started, as earlier noted, weaker already in March 2007 (CR 2054), was intensified in August 2007 (CR 2060), lasting with some variations in amplitude, but with stable period, until November 2008 (CR 2077). Figure 4d also shows that the second and, especially, the third harmonics were strong in SW velocity at times
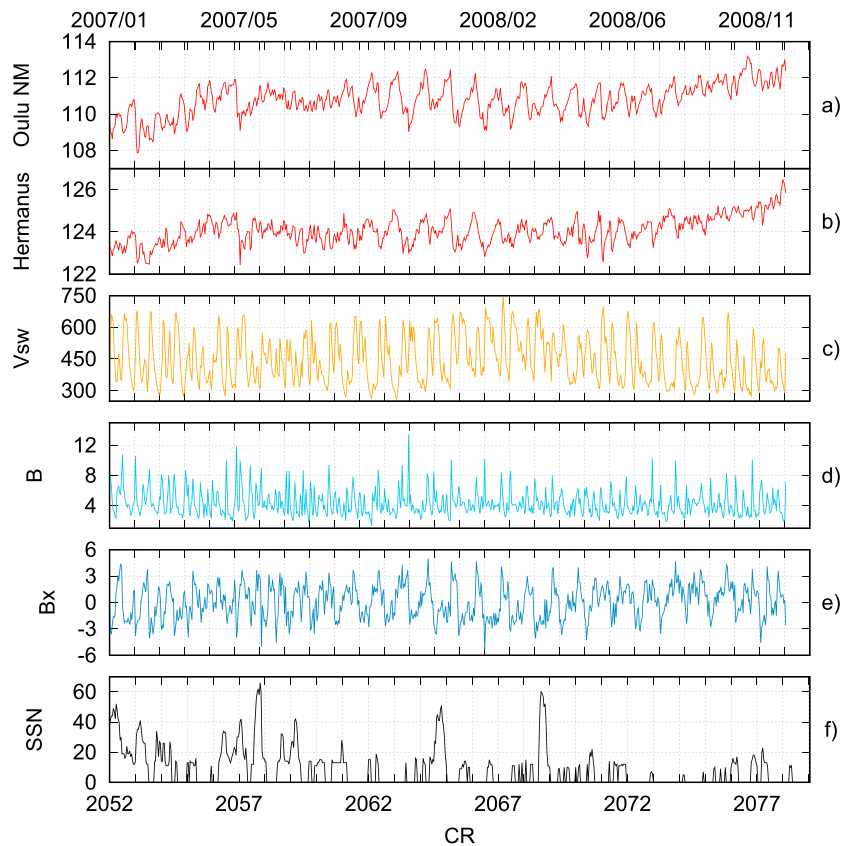
Figure 2. Five-day running means of daily (a) Oulu and (b) Hermanus cosmic ray NM count rates; (c) solar wind velocity (Vsw); (d) strength of the heliospheric magnetic field (*B*), (e) HMF Bx component; and (f) sunspot number (SSN) in 2007–2008 (CRs 2052–2078). Time is given in Carrington rotations (CR) below and in calendar months above. NM = neutron monitors; HMF = heliospheric magnetic field.

of reduced 27-day power, in agreement with earlier findings (Love et al., 2012). Similarly as in 2014–2015 solar rotation periodicity was only weakly present in the HMF strength in 2007–2008.

In order to study the main periodicities more precisely, we calculated the power spectrum densities (PSDs) of the same three parameters using Lomb-Scargle algorithm (Lomb, 1976; Scargle, 1981). Figure 5 presents the PSDs for these parameters for the two intervals of main rotation activity: Interval A, 13 August 2014 to 3 March 2015 and Interval B, 22 September 2007 to 16 June 2008. The exact values of the dominant periodicity for these and a few other parameters are given in Table 1. The main periodicity in CR intensity in Interval A for both stations was 28.9 days. However, the main periodicity for other parameters of this time interval were
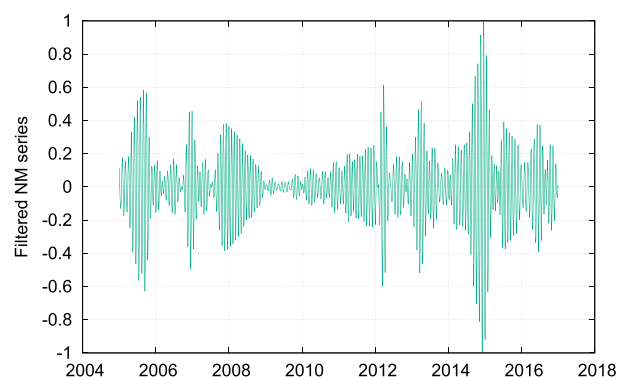

Figure 3. Daily NM count rates of Oulu station in 2005–2016 bandpass filtered to (29 ± 5) days. NM = neutron monitors.
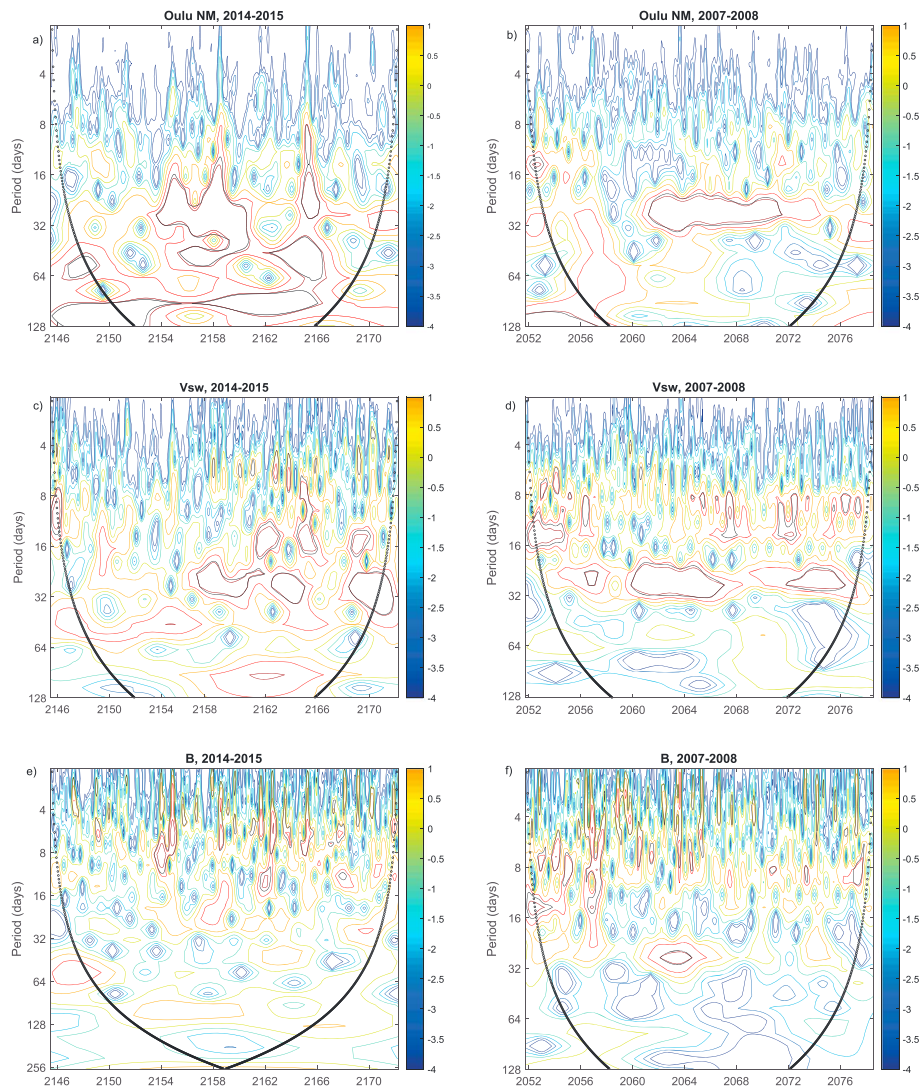
Figure 4. Wavelet analysis for (a, b) Oulu NM, (c, d) solar wind velocity, and (e, f) HMF strength in 2014–2015 and 2007–2008. The x axis gives time in Carrington rotations. NM = neutron monitors; HMF = heliospheric magnetic field.

shorter: 26.1 days for SW velocity and 26.9 days for HMF Bx component. For HMF strength the main periodicity was 7.8 days and for sunspots 20.2 days.

In Interval B the main periodicity in cosmic rays intensity for both NMs was 27.5 days. Note that exactly the same periodicity was also found for SW velocity. A bit shorter periodicity of 26.8 days characterized HMF Bx component and sunspot number. In HMF strength (Figure 5f) the strongest was the third harmonic period of 9.1 days, but the first harmonic of 27.5 days was only slightly weaker. Figure 5d further verifies that the second and the third harmonics of the SW velocity (13.6 and 9.1 days) were quite strong in 2007–2008 (e.g., Modzelewska & Alania, 2013).

4. Fourier Series Amplitudes and Phases

We have also calculated the amplitudes A_k and phases φ_k of the harmonic variation of the three parameters for each solar rotation in Interval A and Interval B. The Fourier series for parameter $x(t)$ is calculated as follows (e.g., Gil & Mursula, 2017; Xue & Chen, 2008):

$$x(t_n) = \frac{a_0}{2} + \sum_{k=1}^{T/2} \left(a_k \cos \frac{2\pi k t_n}{T} + b_k \sin \frac{2\pi k t_n}{T} \right) = \frac{a_0}{2} + \sum_{k=1}^{T/2} \left(A_k \sin \left(\frac{2\pi k t_n}{T} + \varphi_k \right) \right), \tag{1}$$
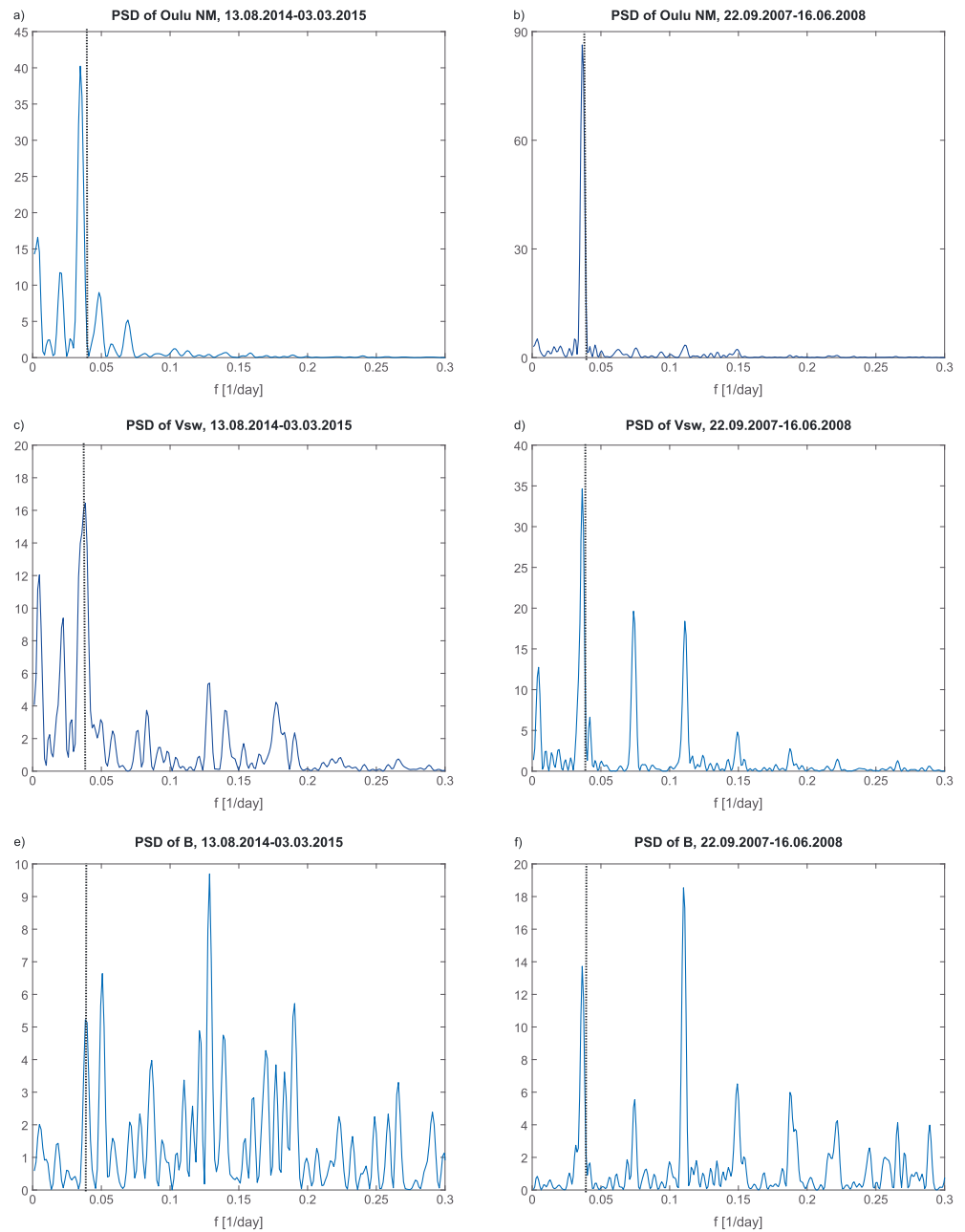
Figure 5. PSD of (a, b) Oulu NM, (c, d) solar wind velocity, and (e, f) HMF strength (*B*) data in Interval A (13 August 2014 to 3 March 2015) and in Interval B (22 September 2007 to 16 June 2008); *x* axis depicts frequency in unit of 1/day. Dotted vertical line marks the frequency corresponding to the period of exactly 27 days. PSD = power spectrum density; NM = neutron monitor; HMF = heliospheric magnetic field.

where

$$a_k = \frac{1}{T/2} \sum_{n=1}^{T} x(t_n) \cos \frac{\pi k t_n}{T/2} \qquad (2)$$

and

$$b_k = \frac{1}{T/2} \sum_{n=1}^{T} x(t_n) \sin \frac{\pi k t_n}{T/2} \qquad (3)$$

Table 1
The Most Significant Periods (in days) for Six Parameters in Interval A (13 August 2014 to 3 March 2015) and Interval B (22 September 2007 to 16 June 2008)

Parameter	Period Interval A	Period Interval B
Oulu NM	28.9	27.5
Hermanus NM	28.9	27.5
Solar wind velocity	26.1	27.5
HMF strength	7.8	9.1
HMF Bx component	26.9	26.8
Sunspot number	20.2	26.8

Note. NM = neutron monitor; HMF = heliospheric magnetic field.

are the Fourier coefficients, and $x(t_n)$ denotes the daily data for parameter x. We have used here a fixed value of $T = 27$ days for solar rotation, but for cosmic rays in 2014–2015 we take $T = 29$ days and for SW velocity in 2014–2015 $T = 26$ days, based on Table 1. We give the mean amplitudes of Oulu NM, SW velocity and HMF strength for the two intervals in Table 2. We found that the amplitude for cosmic rays was indeed far greater in Interval A than Interval B for both NM stations. On the other hand, the amplitudes of SW velocity and HMF strength were slightly lower in Interval A than in Interval B.

Figures 6a and 6b show the corresponding recurrence phases for Oulu NM, SW velocity and HMF strength for the two intervals. In Interval B the phase of cosmic ray intensity was very stable, as expected from Figures 4 and 5. During the time when the recurrence was simultaneously strong in SW velocity and cosmic ray intensity (CRs 2062–2066), they were almost in antiphase. At this time the phase of HMF strength was also quite stable but some 40° (220°) ahead of the phase of SW velocity (cosmic rays). Note that the observed phase difference between SW velocity and HMF strength corresponds to a typical time delay of 2–3 days between a HMF compression of a CIR and the subsequent SW velocity maximum. The relative phase between SW velocity and HMF strength varied over time only relatively weakly and always remains in the same order. However, toward the end of Interval B, when SW speed amplitude decreased, the relative phase between Oulu NM and HMF strength decreased to roughly opposite (180°). At this time the amplitude of HMF variation was largest, as seen in Figure 4f. This indicates that the HMF enhancement produced by the compression effect of the high-speed wind dominated GCR modulation at this time.

In Interval A the phase pattern was very different from the 2007–2008 interval. Oulu NM depicted a somewhat less systematic behavior, with larger range phase values. The same applied for SW velocity and HMF strength. However, most dramatically the relative phase between Oulu NM and SW velocity showed no define organization, being sometimes negative and sometimes positive. Moreover, during CR 2157, when both parameters depicted the largest rotation amplitude, the relative phase was close to 0. Note also that although the HMF strength amplitude was weak, the relative phase between SW velocity and HMF strength followed the same CIR-expected pattern over most of the interval.

5. Wavelet Coherence

The above results show the spectral content of the studied parameters but not their detailed mutual relationships in time-frequency space. In order to further study the interdependence between the different

Table 2
Average Amplitudes of Recurrence for Oulu and Hermanus NMs, Solar Wind Velocity, and the HMF Strength Using Fixed T in Interval A (13 August 2014 to 3 March 2015) and Interval B (22 September 2007 to 16 June 2008)

Parameter	Interval A				Interval B			
	Oulu NM	HERM NM	Vsw	B	Oulu NM	HERM NM	Vsw	B
Period T	29	29	26	27	27	27	27	27
Amplitude	2.14	1.93	0.15	0.16	0.82	0.45	0.20	0.19

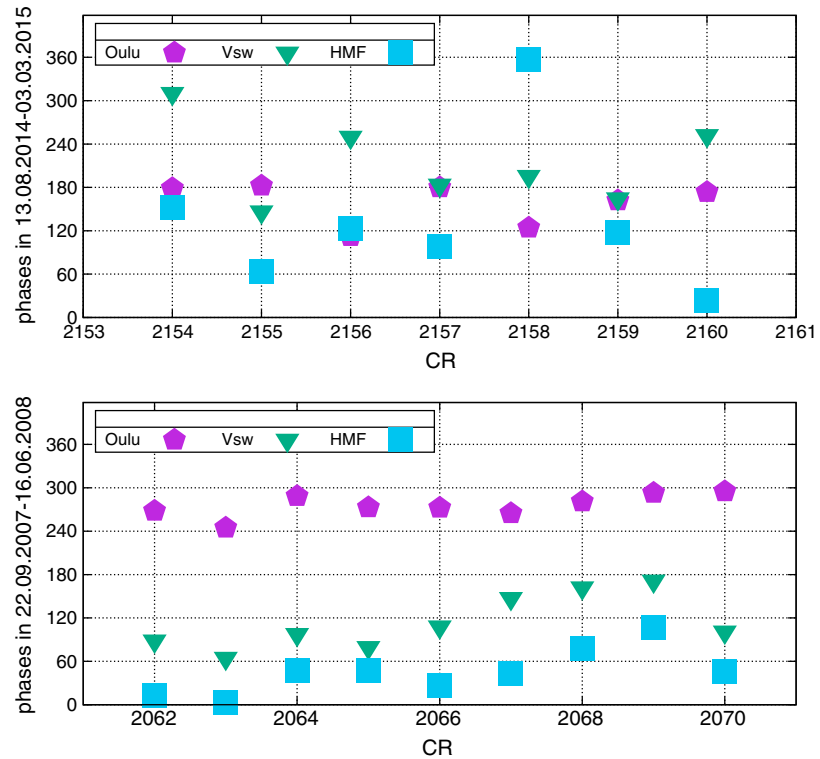*Note.* NM = neutron monitor; HERM = Hermanus.

Figure 6. Recurrence phases for Oulu NM (purple pentagons), solar wind velocity (green triangles), and HMF strength (blue squares) for each solar rotation in the two intervals, A: 13 August 2014 to 3 March 2015 (top) and B: 22 September 2007 to 16 June 2008 (bottom). The *x* axis gives the time in CR. NM = neutron monitor; HMF = heliospheric magnetic field; CR = Carrington rotations.

parameters, we calculated the crosswavelet spectrum for GCR and Vsw, as well as for GCR and HMF strength, using the corresponding wavelet transforms W_{GCR}, W_{Vsw}, and W_B in the form (Torrence & Compo, 1998)

$$W_{GCR,x} = W_{GCR}W_x^*, \tag{4}$$

where *x* denotes Vsw or *B*, and * denotes complex conjugation. The crosswavelet power is $|W_{GCR,x}|$ and the phase angle gives the phase relationship between GCR and the other parameter (Jevrejeva et al., 2003). The crosswavelet spectra computed using the tools introduced by Jevrejeva et al. (2003) and Grinsted et al. (2004) are displayed in Figure 7. Figure 7a shows that there was a period at the end of 2014 and the beginning of 2015 (CRs 2157–2160) when cosmic rays and SW velocity had stable phase difference and when the common power was strong and statistically significant (95 % significance marked with thin black line in the figures). In 2007–2008 cosmic rays and SW velocity were nearly perfectly in antiphase (arrows directed to the left) during the whole period of enhanced recurrent variability (Figure 7b), with strong and statistically significant mutual power. Figure 7c shows that in 2014–2015 there was no stable phase difference between cosmic rays and HMF strength, but there was a period at the end of 2014 and beginning of 2015 (CRs 2157–2160) where we can observe a statistically significant common power. On the other hand, at the end of 2007 and beginning of 2008 (CRs 2062–2067) there was also a period of statistically significant mutual power of GCR and *B* with a stable phase difference of about 230° (Figure 7d).

Next, following Grinsted et al. (2004), we calculated the wavelet coherence, which is a measure of covariance intensity in time-frequency space (e.g., Koopmans, 2014). Wavelet coherence is defined as follows (Torrence & Webster, 1999):

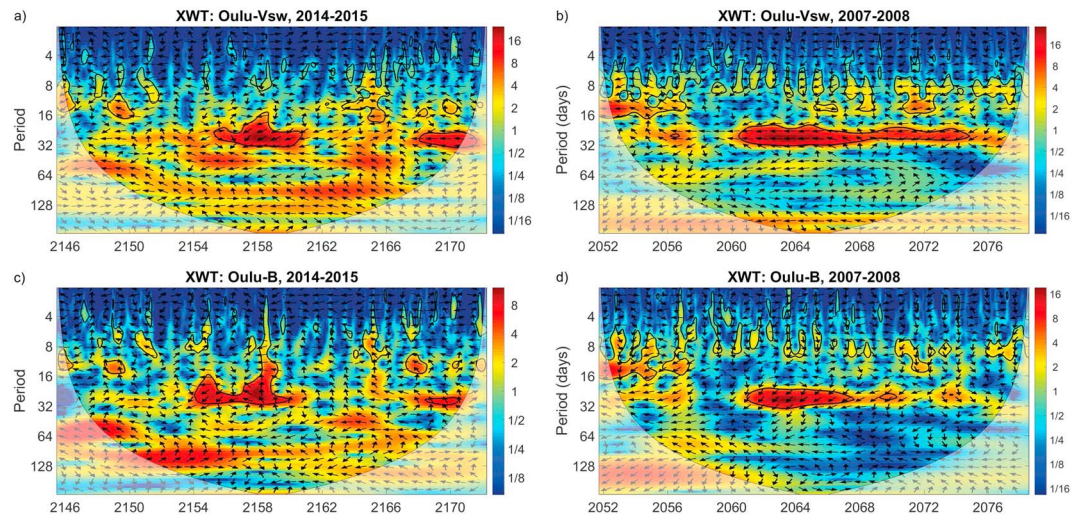$$R^2 = \frac{|S(W_{GCR,x}/s)|^2}{|S(W_{GCR}/s)|^2 \cdot |S(W_x/s)|^2}, \tag{5}$$

Figure 7. Cross wavelet transform of (a, b) Oulu neutron monitor and Vsw; (c, d) Oulu neutron monitor and HMF strength (*B*) data in 2014–2015 (a, c) and in 2007–2008 (b, d). The *x* axis gives the time in Carrington rotations. Arrows indicate the relative phase between the two parameters, with right (left) arrow indicating correlation (anticorrelation) and upward (downward) arrow that the first parameter is lagging (leading) the second by 90°. HMF = heliospheric magnetic field.

where operator S denotes smoothing and s the wavelet scale. Wavelet coherence (WTC) is a measure of local correlation between the two continuous wavelet transforms (in our case between cosmic rays intensity and SW velocity or HMF strength), indicating possible coherence even when the common power is weak (Grinsted et al., 2004).

The results for wavelet coherence are given in Figure 8. Coherence between GCR and SW velocity, in the range of variability related to solar rotation, was more robust and lasted longer in 2007–2008 than in 2014–2015. This is related to the above mentioned fact that GCR and Vsw had exactly the same dominant period in 2007–2008 but not in 2014–2015 (see Table 1). Figure 8b further verifies that in 2007–2008 SW velocity and cosmic rays were almost perfectly in antiphase, while in 2014–2015 (Figure 8a) their mutual phase difference was varying, from being in antiphase up to about 130° difference. Figure 8 also verifies the above results that
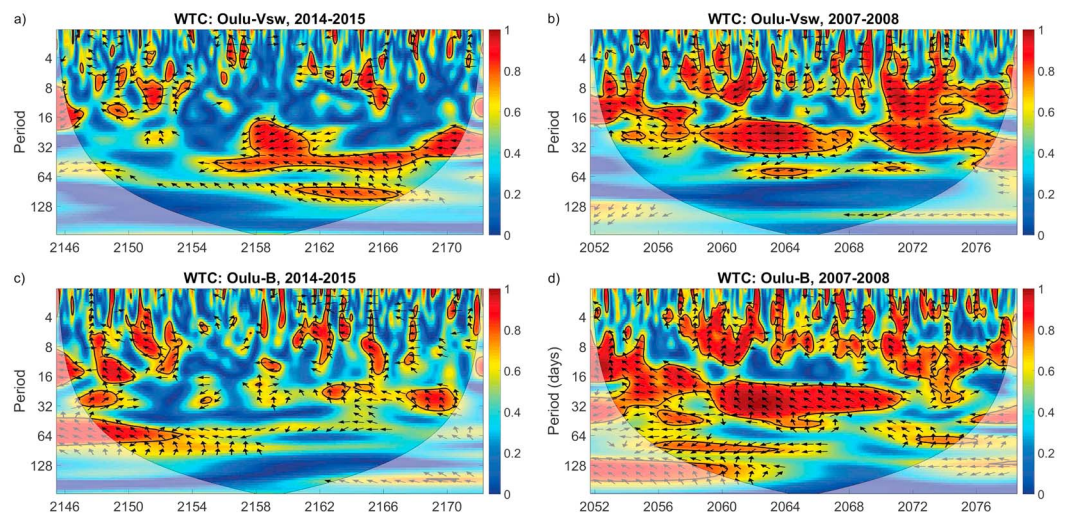

Figure 8. Wavelet coherence for (a, b) Oulu neutron monitor and Vsw; (c, d) Oulu neutron monitor and HMF strength (*B*) data in 2014–2015 (a, c) and in 2007–2008 (b, d). The *x* axis gives the time in Carrington rotations. Arrows indicate the relative phase between the two parameters, with right (left) arrow indicating correlation (anticorrelation) and upward (downward) arrow that the first parameter is lagging (leading) the second by 90°. HMF = heliospheric magnetic field.
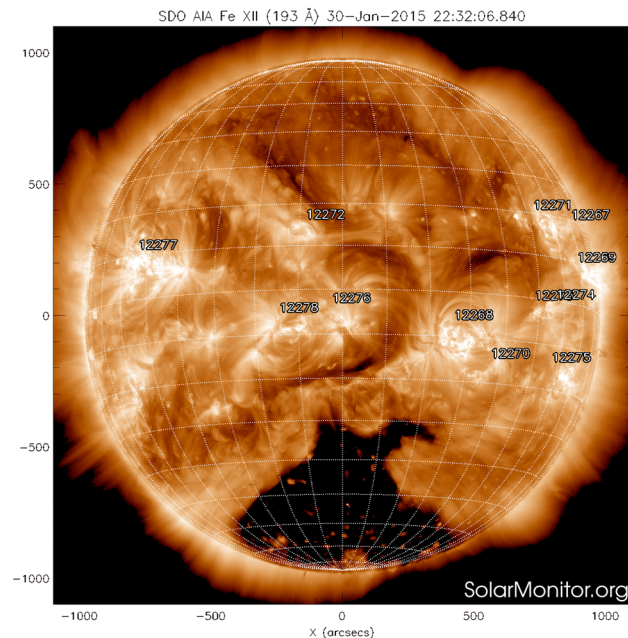
Figure 9. Polar coronal hole on 30 January 2015. Source: https://www.solarmonitor.org.

in 2014–2015 there were only short time intervals with statistically significant coherence between cosmic rays and HMF strength, but in 2007–2008 there was a long interval of significant coherence and a stable phase difference of about 230°.

6. Discussion

It is well known that solar rotation recurrence of cosmic ray intensity is related to CHs and their development in time (e.g., Kunow et al., 1995). They modify the structure of SW by producing high-speed streams, which can effectively affect GCR by convection, thus modulating the GCR flux at solar rotation rate. At times when there exists one large CH at low latitudes, or a polar CH extends to low latitudes, the basic harmonic of solar rotation rate is enhanced in GCR recurrence. Kota and Jokipii (2001) studied effects of nonpolar CHs on cosmic-ray transport. Using a three-dimensional mathematical model, they found that depressions in GCR flux are produced by the high-speed streams. Earlier, Burlaga et al. (1984) indicated that GCR flux decreases are related to transient systems, while GCR increases are connected to corotating structures. Similar results were obtained by Kota and Jokipii (1991) based on mathematical modeling. Alania and coauthors (e.g., Gil & Alania, 2013) have shown that near solar minimum the 27-day variation of GCR is connected with SW speed changes, while near solar maximum it is rather connected to HMF strength variability.

We have considered here the two time intervals, Interval A and Interval B, when GCR fluxes depicted the strongest variation at solar rotation period, during the last two solar cycles. We have analyzed the full-disk extreme ultraviolet images obtained by Solar and Heliospheric Observatory Extreme ultraviolet Imaging Telescope and by Solar Dynamics Observatory Atmospheric Imaging Assembly before and during these two intervals. In Interval A we found a large CH in the Southern Hemisphere about 3–4 days before each decrease in cosmic ray intensity. One example of CH for that interval is presented in Figure 9. This CH produced quite a broad peak in power spectrum density of cosmic ray intensity (Figure 5a) with the maximum at a rather long period of about 28.9 days (see Table 1). This period is clearly longer than the period in Interval B, when the power peak was also narrower (see Figure 5d). Values of the average amplitudes (Table 2) and behavior of the phases (Figure 6) of solar rotation rate variability of cosmic rays, SW velocity, and heliospheric magnetic field strength suggest that the CH causing the enhanced solar rotation rate recurrence was at a different heliolatitude having a different longitudinal distribution. In both cases, the polar CHs in the two hemispheres were very different, which led to a very asymmetric magnetic configuration at middle to low heliospheric latitudes and to a strong recurrence at the solar rotation rate. The convection effect by high-speed SW is the likely source of the strong periodicity in cosmic rays.
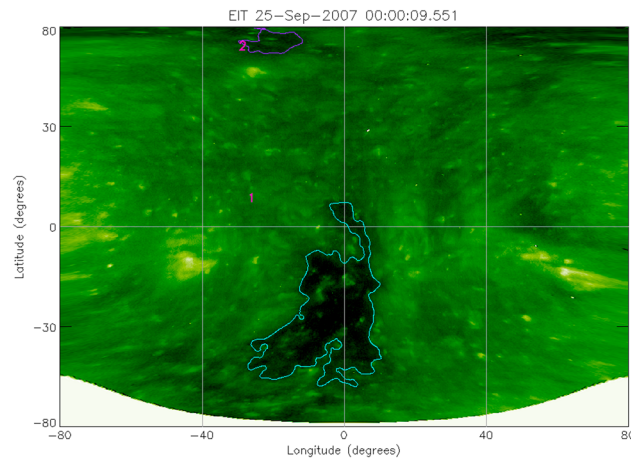
Figure 10. Coronal hole on 25 September 2007. Source: http://umbra.nascom.nasa.gov.

Lowder et al. (2017) and Hamada et al. (2018) found a difference in the evolution of northern and southern CHs during the SC 23 and SC 24. In Interval B the polar CHs were not as large as in Interval A, but there were low-latitude CHs (Figure 10), even with transequatorial extensions (e.g., Dunzlaff et al., 2008; Gómez-Herrero et al., 2009), which caused the narrow peak in power spectrum density of 27.5 days in GCR. Kryakunova et al. (2015) noted that the high-speed SW streams from the low-latitude CHs caused the recurrence in 2007. Comparing Figures 9 and 10 shows a clear difference in the latitudinal location and longitudinal distribution of CHs during the two analyzed time intervals and explains the difference in the main periods (28.9 days for 2014–2015 and 27.5 days for 2007–2008) of CR variability. In 2014–2015 the main sources of high Vsw and GCR recurrence were at different heliolatitudes, but in 2007–2008 they were at the same (low) heliolatitude.

7. Summary

During the early declining phase of solar cycle 24, from August 2014 to March 2015 (CRs 2154–2162, Interval A), GCR intensity measured by neutron monitors with widely different cutoff rigidities, presented a very strong variability at a rather long solar rotation period of 28.9 days. SW velocity and HMF Bx component were modulated at a clearly shorter period of 26.1 and 26.9 days, respectively, over partially overlapping time interval. The enhanced solar rotation periodicity in cosmic rays was related to the large and longitudinally asymmetric structure of the southern polar CH covering a wide range of latitudes. This structure led to a strongly asymmetric magnetic configuration in the heliosphere and to the observed differences in the periodicities between different parameters.

Another interval of greatly enhanced recurrence of cosmic rays at the solar rotation period took place from September 2007 to June 2008 (CRs 2061–2073, Interval B). However, in this case the cosmic ray recurrence period was shorter, about 27.5 days. Moreover, in this case the SW velocity depicted exactly the same recurrence period as cosmic rays, and the time interval of the recurrence was closely similar for the two parameters. In this case a low-latitude CH caused the exceptional recurrence of both parameters.

Thus, in both cases the source of variability for cosmic rays and SW velocity were CHs, but the CHs were very different during these two time intervals. While a strongly north-south asymmetric polar CH existed in Interval A, a transequatorial CH extension dominated recurrence in Interval B. This shows that CHs at different heliolatitudes can modulate the flux of cosmic rays. In Interval A the CH covered a wide range of latitudes from the southern pole up to midlatitudes, leading to a broad peak in power spectrum density of cosmic rays, with the main period at 28.9 days. In Interval B, when a CH was at low latitudes (nearly transequatorial), the power spectrum was narrower and the period was shorter.

We would also like to note that in Interval A the solar polarity had just reversed from negative to positive, enhancing the effect of convection by the high-speed streams from southern polar CH to the drifting GCRs. On the other hand, in Interval B solar polarity was negative and the cosmic rays were drifting inward via the heliospheric current sheet. Then, a low-latitude CH could make the current sheet deviate at that longitude and

reduce the cosmic ray flux locally. Accordingly, the physical mechanisms of CH affecting cosmic rays are somewhat different in the two studied cases: convection in 2014–2015 and convection and heliospheric current sheet structure in 2007–2008.

References

Abramenko, V., Yurchyshyn, V., Linker, J., Mikić, Z., Luhmann, J., & Lee, C. O. (2010). Low-latitude coronal holes at the minimum of the 23rd solar cycle. *The Astrophysical Journal*, *712*, 813–818.

Bazilevskaya, G. A., Cliver, E. W., Kovaltsov, G. A., Ling, A. G., Shea, M. A., Smart, D. F., & Usoskin, I. G. (2014). Solar cycle in the heliosphere and cosmic rays. *Space Science Reviews*, *186*, 409–435.

Burlaga, L. F., McDonald, F. B., Ness, N. F., Schwenn, R., Lazarus, A. J., & Mariani, F. (1984). Interplanetary flow systems associated with cosmic ray modulation in 1977–1980. *Journal of Geophysical Research*, *89*, 6579–6587. https://doi.org/10.1029/JA089iA08p06579

Dunzlaff, P., Heber, B., Kopp, A., Rother, O., Müller-Mellin, R., Klassen, A., et al. (2008). Observations of recurrent cosmic ray decreases during solar cycles 22 and 23. *Annales Geophysicae*, *26*, 3127–3138.

Gil, A., & Alania, M. V. (2013). Theoretical and experimental studies of the rigidity spectrum of the 27-day variation of the galactic cosmic ray intensity in different epochs of solar activity. *Solar Physics*, *283*, 565–578.

Gil, A., & Mursula, K. (2017). Hale cycle and long-term trend in variation of galactic cosmic rays related to solar rotation. *Astronomy and Astrophysics*, *599*, A112.

Gómez-Herrero, R., Klassen, A., Müller-Mellin, R., Heber, B., Wimmer-Schweingruber, R., & Böttcher, S. (2009). Recurrent CIR-accelerated ions observed by STEREO SEPT. *Journal of Geophysical Research*, *114*, A05101. https://doi.org/10.1029/2008JA013755

Grinsted, A., Moore, J. C., & Jevrejeva, S. (2004). Application of the cross wavelet transform and wavelet coherence to geophysical time series. *Nonlinear Processes in Geophysics*, *11*, 561ȦŞ–566.

Guo, X., & Florinski, V. (2014). Corotating interaction regions and the 27 day variation of galactic cosmic rays intensity at 1 AU during the cycle 23/24 solar minimum. *Journal of Geophysical Research: Space Physics*, *119*, 2411–2429. https://doi.org/10.1002/2013JA019546

Hamada, A., Asikainen, T., Virtanen, I., & Mursula, K. (2018). Automated identification of coronal holes from synoptic EUV maps. *Solar Physics*, *293*(71), 26.

Hoeksema, J. T. (2010). Evolution of the large-scale magnetic field over three solar cycles. In A. G. Kosovichev, A. H. Andrei, & J.-P. Rozelot (Eds.), *Solar and stellar variability: Impact on Earth and planets, IAU Symposium* (Vol. 264, pp. 222–228).

Jevrejeva, S., Moore, J. C., & Grinsted, A. (2003). Influence of the Arctic oscillation and El Nino-Southern Oscillation (ENSO) on ice conditions in the Baltic Sea: The wavelet approach. *Journal of Geophysical Research*, *108*(D21), 4677.

Jian, L. K., Russell, C. T., & Luhmann, J. G. (2011). Comparing solar minimum 23/24 with historical solar wind records at 1 AU. *Solar Physics*, *274*, 321–344.

Kanasewich, E. E. (1981). *Time sequence Analysis in geophysics*. Edmonton, Alberta, Canada: The University of Alberta Press.

Kirk, M. S., Pesnell, W. D., Young, C. A., & Hess Webber, S. A. (2009). Automated detection of EUV polar coronal holes during solar cycle 23. *Solar Physics*, *257*, 99–112.

Koopmans, L. H. (2014). *The spectral analysis of time series: Probability and mathematical statistics*. Cambridge, MA: Academic Press.

Kota, J., & Jokipii, J. R. (1991). The role of corotating interaction regions in cosmic-ray modulation. *Geophysical Research Letters*, *18*, 1797–1800.

Kota, J., & Jokipii, J. R. (2001). Cosmic ray transport in a heliospheric magnetic field with non-polar coronal holes. *Space Science Reviews*, *97*, 327–330.

Kraaikamp, E., & Verbeeck, C. (2015). Solar demon—An approach to detecting flares, dimmings, and EUV waves on SDO/AIA images. *Journal of Space Weather and Space Climate*, *5*(27), A18.

Kryakunova, O., Belov, A., Abunin, A., Abunina, M., Eroshenko, E., Malimbayev, A., et al. (2015). Recurrent and sporadic Forbush-effects in deep solar minimum. *Journal of Physics Conference Series*, *632*, 012062.

Kunow, H., Dröge, W., Heber, B., Müller-Mellin, R., Röhrs, K., Sierks, H., et al. (1995). High energy cosmic-ray nuclei results on Ulysses: 2. Effects of a recurrent high-speed stream from the southern polar coronal hole. *Space Science Reviews*, *72*, 397–402.

Kunow, H., Wibberenz, G., Green, G., Müller-Mellin, R., & Kallenrode, M.-B. (1991). Energetic particles in the inner solar system. In R. Schwenn & E. Marsch (Eds.), *Physics of the inner heliosphere* (Vol. 2, pp. 243–342) Berlin: Springer-Verlag.

Lario, D., & Roelof, E. C. (2007). Energetic particles during the first and third Ulysses southern high-latitude excursions: Probing global corotating interaction region structure beyond 5 AU. *Journal of Geophysical Research*, *112*, A09107. https://doi.org/10.1029/2007JA012414

Leske, R., Cummings, A. C., Mewaldt, R. A., Stone, E. C., von Rosenvinge, T. T., & Wiedenbeck, M. E. (2011). Observed 27-day variations in cosmic ray intensities during the cycle 23/24 solar minimum. *Proceedings of the 32nd ICRC2011*, *11*, 194–197. https://doi.org/10.7529/ICRC2011/V11/0721

Lingri, D., Mavromichalaki, H., Belov, A., Eroshenko, E., Yanke, V., Abunin, A., & Abunina, M. (2016). Forbush decreases during the DeepMin and MiniMax of solar cycle 24. ArXiv e-prints 1612.08900.

Lomb, N. R. (1976). Least-squares frequency analysis of unequally spaced data. *Astrophysics and Space Science*, *39*, 447–462.

Love, J. J., Joshua Rigler, E., & Gibson, S. E. (2012). Geomagnetic detection of the sectorial solar magnetic field and the historical peculiarity of minimum 23–24. *Geophysical Research Letters*, *39*, L04102. https://doi.org/10.1029/2011GL050702

Lowder, C., Qiu, J., & Leamon, R. (2017). Coronal holes and open magnetic flux over cycles 23 and 24. *Solar Physics*, *292*, 18.

McComas, D. J., Ebert, R. W., Elliott, H. A., Goldstein, B. E., Gosling, J. T., Schwadron, N. A., & Skoug, R. M. (2008). Weaker solar wind from the polar coronal holes and the whole Sun. *Geophysical Research Letters*, *35*, L18103. https://doi.org/10.1029/2008GL034896

Mewaldt, R. A., Davis, A. J., Lave, K. A., Leske, R. A., Stone, E. C., Wiedenbeck, M. E., et al. (2010). Record-setting cosmic-ray intensities in 2009 and 2010. *The Astrophysical Journal*, *723*, L1–L6.

Modzelewska, R., & Alania, M. V. (2013). The 27-day cosmic ray intensity variations during solar minimum 23/24. *Solar Physics*, *286*, 593–607.

Monk, A. T., & Compton, A. H. (1939). Recurrence phenomena in cosmic-ray intensity. *Reviews of Modern Physics*, *11*, 173–179.

Moraal, H., & Stoker, P. H. (2010). Long-term neutron monitor observations and the 2009 cosmic ray maximum. *Journal of Geophysical Research*, *115*, A12109. https://doi.org/10.1029/2010JA015413

Parker, E. N. (1956). Modulation of primary cosmic-ray intensity. *Physical Review*, *103*, 1518–1533.

Picozza, P., Galper, A. M., Castellini, G., Adriani, O., Altamura, F., Ambriola, M., et al. (2007). PAMELA: A payload for antimatter matter exploration and light-nuclei astrophysics. *Astroparticle Physics*, *27*, 296–315.

Richardson, I. G. (2004). Energetic particles and corotating interaction regions in the solar wind. *Space Science Reviews*, *111*, 267–376.

Scargle, J. D. (1981). Studies in astronomical time series analysis. I—Modeling random processes in the time domain. *Astrophysical Journal Supplement Series*, *45*, 1–71.

Shenoi, B. A. (2005). *Introduction to Digital Signal Processing and Filter Design*. Hoboken, NJ: John Wiley.

Simpson, J. A. (2000). The cosmic ray nucleonic component: The invention and scientific uses of the neutron monitor (keynote lecture). *Space Science Reviews*, *93*, 11–32.

Singh, Y. P., & Badruddin (2017). Short- and mid-term oscillations of solar, geomagnetic activity and cosmic-ray intensity during the last two solar magnetic cycles. *Planeary and Space Science*, *138*, 1–6.

Stone, E. C., Cohen, C. M. S., Cook, W. R., Cummings, A. C., Gauld, B., Kecman, B., et al. (1998). The cosmic-ray isotope spectrometer for the Advanced Composition Explorer. *Space Science Reviews*, *86*, 285–356.

Suzuki, M. (2014). On the long-term modulation of solar differential rotation. *Solar Physics*, *289*, 4021–4029.

Torrence, C., & Compo, G. P. (1998). A practical guide to wavelet analysis. *Bulletin of the American Meteorological Society*, *79*, 61–78.

Torrence, C., & Webster, P. J. (1999). Interdecadal changes in the ENSO-monsoon system. *Journal of Climate*, *12*, 2679–2690.

Xue, D., & Chen, Y. (2008). *Solving Applied Mathematical Problems with MATLAB*. Boca Raton, FL: CRC Press.

Zhang, L., Mursula, K., & Usoskin, I. (2013). Consistent long-term variation in the hemispheric asymmetry of solar rotation. *Astronomy & Astrophysics*, *552*, A84.